Journal of Power Sources 196 (2011) 62–68

Contents lists available at ScienceDirect

Journal of Power Sources

journal homepage: www.elsevier.com/locate/jpowsour

A novel electronic current-blocked stable mixed ionic conductor for solid oxide fuel cells

Wenping Sun[a], Yinzhu Jiang[b], Yanfei Wang[c], Shumin Fang[d], Zhiwen Zhu[a], Wei Liu[a,*]

[a] CAS Key Laboratory of Materials for Energy Conversion, Department of Materials Science and Engineering, University of Science and Technology of China (USTC), Hefei 230026, PR China
[b] State Key Laboratory of Silicon Materials, Department of Materials Science and Engineering, Zhejiang University, Hangzhou, Zhejiang 310027, PR China
[c] Department of Chemistry, University of Science and Technology of China (USTC), Hefei 230026, PR China
[d] Inorganic Membranes, Faculty of Science and Technology, MESA+ Institute for Nanotechnology, University of Twente, P.O. Box 217, 7500 AE, Enschede, The Netherlands

ARTICLE INFO

Article history:
Received 29 May 2010
Received in revised form 12 July 2010
Accepted 13 July 2010
Available online 21 July 2010

Keywords:
Mixed ionic conductor
Electrolyte
Electronic current-blocked
Electrochemical performance
Solid oxide fuel cells

ABSTRACT

A novel ionic conductor, $BaCe_{0.8}Sm_{0.2}O_{3-\delta}$–$Ce_{0.8}Sm_{0.2}O_{2-\delta}$ (BCS–SDC, weight ratio 1:1), is reported as an electrolyte material for solid oxide fuel cells (SOFCs). Homogeneous BCS–SDC composite powders are synthesized via a one-step gel combustion method. The BCS and SDC crystalline grains play a role as matrix for each other in the composite electrolyte. The composite avoids the typical drawbacks of BCS and SDC, showing not only a better chemical stability than the single phase of BCS but much higher open circuit voltages (OCVs) than the single phase of SDC under the fuel cell conditions. Moreover, BCS–SDC exhibits mixed oxygen ionic and protonic conduction. A total conductivity of 0.0204 S cm^{-1} at 700 °C is achieved in wet hydrogen (3% H_2O), the value of which is comparable with the state-of-the-art proton conductor $BaZr_{0.1}Ce_{0.7}Y_{0.2}O_{3-\delta}$ (BZCY). The peak power density achieves 505 mW cm^{-2} at 700 °C with a 30-μm-thick BCS–SDC electrolyte using wet H_2 as the fuel. Resistances of the tested cell under open circuit conditions at different operating temperatures are also investigated by impedance spectroscopy.

1. Introduction

Recently, more and more attentions were focused on solid oxide fuel cells (SOFCs) operating at low and/or intermediate temperatures. The decrease of temperature demands an electrolyte with higher ionic conductivity than conventional yttria-stabilized zirconia (YSZ). Both rare earth-doped CeO_2 (DCO, oxygen ionic conductor) and doped $BaCeO_3$ (proton conductor) possess high ionic conductivity at intermediate temperatures and exhibit promising performances in the application of SOFCs [1–9]. DCO is chemically stable in H_2O and CO_2 [10,11] and shows better chemical compatibility with cathode materials [12], which assures the long-term performance stability during operation of SOFCs. However, these materials have some serious drawbacks. In DCO, Ce^{4+} ions can be thermodynamically reduced to Ce^{3+} ions in reducing atmosphere at elevated temperatures, which results in two main problems [13–15], as shown in Fig. 1(a). Firstly, electronic conduction would be introduced in the electrolyte causing internal shorting, remarkable decrease in open circuit voltages (OCVs), and energy loss. Secondly, the chemical expansion coupled with the reduction can generate large stresses and mechanical degradation of the electrolyte [16,17]. Furthermore, the above two problems will be seriously aggravated when increasing operating temperature and/or decreasing electrolyte thickness [18], which severely hampers the practical application of DCO as an electrolyte. On the other side, acceptor-doped $BaCeO_3$, as the current state-of-the-art proton conductor, shows relatively small electronic conductivity but poor chemical stability against H_2O and CO_2 (Fig. 1(b)), limiting its practical applications [19–21]. Even though the chemical stability of $BaCeO_3$ can be improved by substituting partial Ce with Zr or Ta, etc. at the expense of ionic conductivity [5,6,22], it still reacts with CO_2 when exposed in a pure CO_2 atmosphere [21].

Since it is inaccessible to meet all the requirements of electrolyte with a single-phase material, a double-matrix-composite consisting of perovskite-type proton conductor $BaCe_{0.8}Sm_{0.2}O_{3-\delta}$ (BCS) and fluorite-type oxygen ionic conductor $Ce_{0.8}Sm_{0.2}O_{2-\delta}$ (SDC) (BCS–SDC, weight ratio 1:1) is proposed as an electrolyte for SOFCs. With this double-matrix structure, those drawbacks of BCS and SDC can be suppressed and the advantages could be reserved. Fig. 1(c) depicts this double-matrix configuration of the SDC and BCS crystalline grains in the cross-section of the sintered BCS–SDC membrane. The SDC and BCS crystalline grains distribute homogenously in the membranes and play a role as matrix for each other. In this case, BCS grains act as an electron blocking layer across the

* Corresponding author. Tel.: +86 0551 3606929; fax: +86 0551 3602586.
E-mail address: wliu@ustc.edu.cn (W. Liu).

0378-7753/$ – see front matter © 2010 Elsevier B.V. All rights reserved.
doi:10.1016/j.jpowsour.2010.07.038

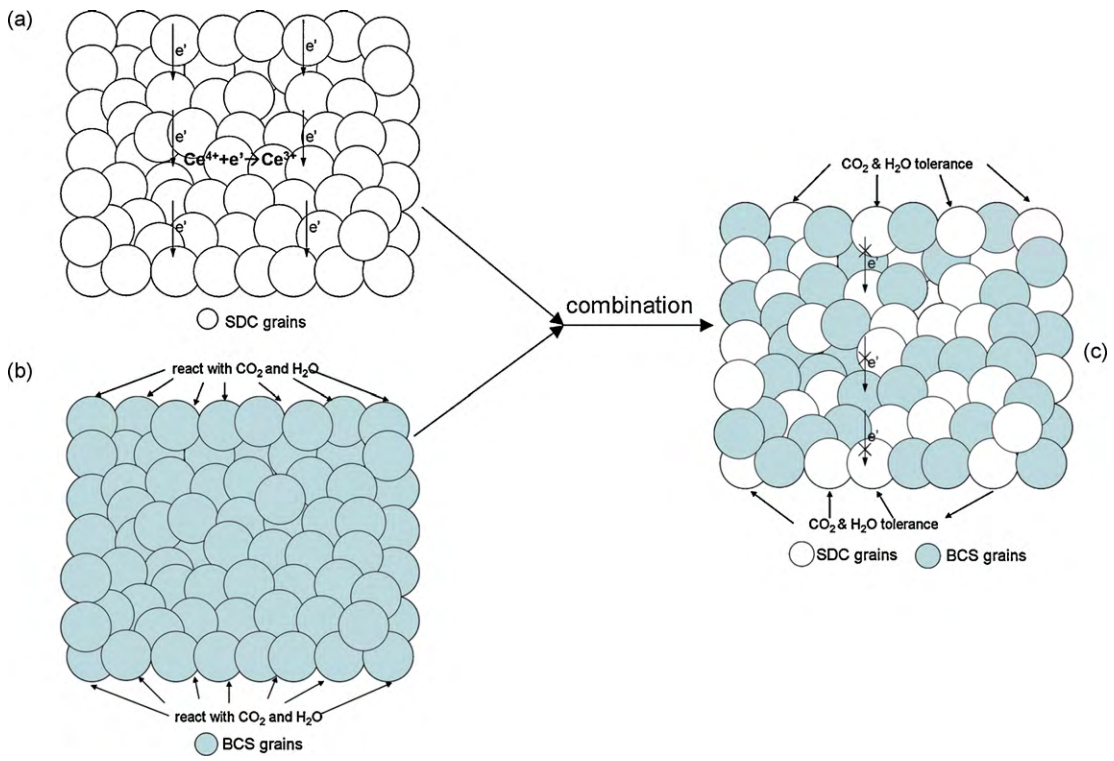

Fig. 1. Schematic description of crystalline grains distributing in the cross-section of the sintered SDC (a), BCS (b), and BCS–SDC (c) membrane.

membrane. That is to say, higher OCVs for BCS–SDC composite can be expected by the fact that the BCS matrix in the composite electrolyte can protect the SDC grains from reduction and hence the electronic conduction in the composite electrolyte would be effectively suppressed. Correspondingly, the mechanical strength could also be improved. On the other hand, the SDC matrix in the composite would act as a covering layer for BCS here, and this can effectively protect BCS grains from corrosion caused by CO_2 and H_2O, leading to a higher chemical stability. Based on this configuration, an electronic current-blocked stable mixed ionic conductor is expected for the application in SOFCs.

In this work, the BCS–SDC double-matrix-composite electrolyte was synthesized via a one-step gel combustion method. The phase structure compared with the two single phases, and the distribution of the two single phases in the composite were investigated. The total electrical conductivity of this novel electrolyte under different atmospheres was determined from the impedance spectra. Moreover, we also evaluate the feasibility of the composite as an electrolyte for SOFCs. The OCVs and long-term stability of the button cells based on the composite electrolyte were studied compared with those typical electrolyte materials. A single cell with a 30-μm-thick BCS–SDC electrolyte was tested using wet H_2 as the fuel, and the electrochemical performance of the cell was also discussed in detail.

2. Experimental

2.1. Powders synthesis and cells fabrication

$BaCe_{0.8}Sm_{0.2}O_{3-\delta}$–$Ce_{0.8}Sm_{0.2}O_{2-\delta}$ (BCS–SDC) composite powders with a weight ratio of 1:1 were synthesized via a one-step gel combustion process [23]. Firstly, Sm_2O_3 was dissolved in HNO_3 under stirring. Then $Ce(NO_3)_3{\cdot}6H_2O$ and $Ba(CH_3COO)_2$ were added into the solution in order. Subsequently, citric acid was introduced with the molar ratio of total metal ions: citric acid at 1:1.5. The pH value was adjusted to about 7 with aqueous ammonia (NH_4OH). The solution was heated and stirred continuously at about 70 °C until gelling. The gel was then moved to an evaporation pan heated on a hot plate. Gel ignition and combustion then occurred, yielding the as-prepared powders. The obtained powders were calcined at 1000 °C for 3 h in air, giving BCS–SDC composite powders. Besides, single-phase BCS and SDC powders were also synthesized via the procedure described above. The anode-supported half cells were fabricated by a co-pressing method and subsequently co-fired at 1350 °C for 5 h. No pore-former (e.g. starch) was introduced in the anode substrate. $Sm_{0.5}Sr_{0.5}CoO_{3-\delta}$–$Ce_{0.8}Sm_{0.2}O_{2-\delta}$ (SSC–SDC) composite was employed as the cathode. The cathode was sintered at 1000 °C for 3 h in air to form a porous cathode layer. Ag paste was applied to the cathode as a current collector.

2.2. Characterization of materials

Phase structures of the powders were identified by X-ray diffraction (XRD) analysis on Philips PW 1730 diffractometer using CuKα radiation. The Raman spectra were measured with a SPEX-1403 Laser Raman spectrometer using a back-scattering technique, and the 541.5 nm line from an argon-ion laser was used as an excitation source. The BCS–SDC pellet used for measuring the conductivity was sintered at 1500 °C for 5 h, and the relative density was greater than 98%. The total conductivity of the sintered pellet between 300 and 750 °C under different atmospheres was studied via a two-point measurement using an impedance analyzer (CHI604B, Shanghai Chenhua) in the frequency range 10^5–1 Hz, and a 5 mV a.c. signal was applied. The sintered pellet was painted with Pt paste on both sides, and then annealed at 900 °C for 1 h to remove the residual organics. Before the measurement, the sample was held for equilibrium at each temperature under all atmospheres. A scanning electron microscopy (SEM, JEOL JSM-6700F) equipped with an energy-dispersive X-ray spectroscopy (EDS) system was used to perform the microstructure and chemical analysis.

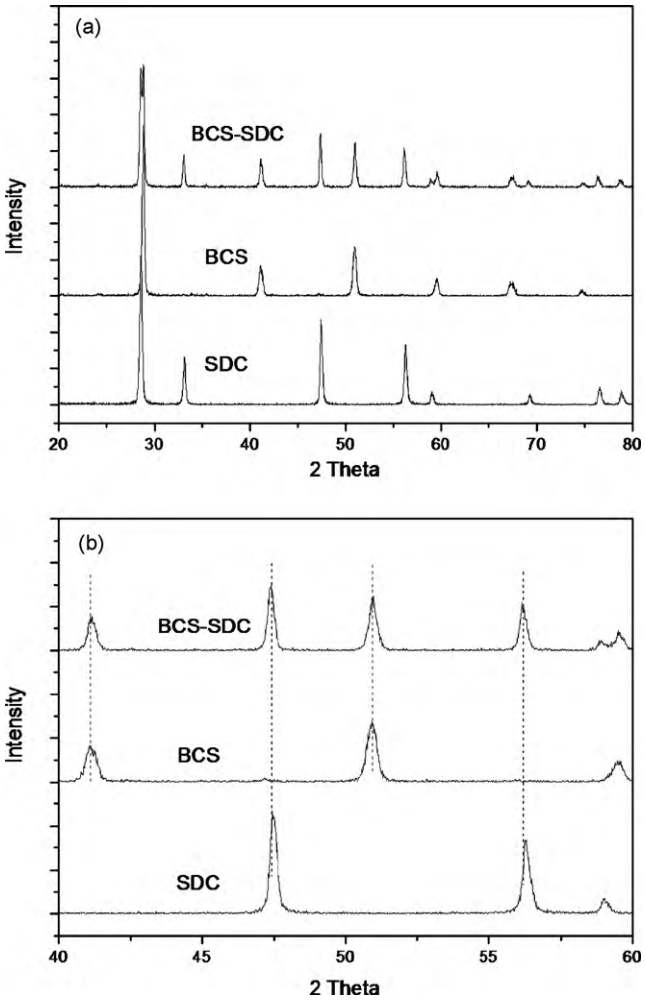

Fig. 2. XRD patterns of the SDC, BCS, and BCS–SDC powder calcined at 1000 °C for 3 h (a) and magnified XRD patterns for $40^\circ \leq 2\theta \leq 60^\circ$ (b).

2.3. Electrochemical measurement of single cells

The button cells were tested in a home-built cell testing system. The cell was tested from 500 to 700 °C using 40 ml min^{-1} humidified hydrogen (3% H_2O) as the fuel and static air as the oxidant. The cell performances were measured with a DC Electronic Load (ITech Electronics model IT8511). The electrochemical impedance spectra of the cell were measured under open current conditions using an impedance analyzer (CHI604B, Shanghai Chenhua) in the frequency range from 0.1 Hz to 100 kHz. Resistances of the cell under open circuit conditions were determined from the impedance spectra.

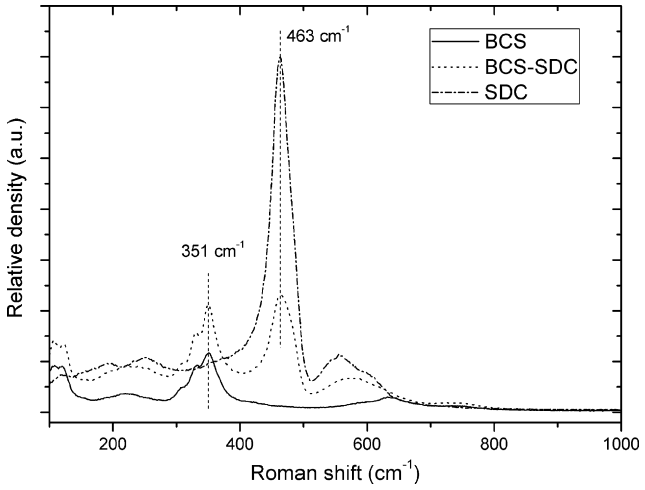

Fig. 3. Raman spectra of the SDC, BCS, and BCS–SDC powder calcined at 1000 °C for 3 h obtained with a 514.5 nm laser line.

3. Results and discussion

Fig. 2 shows the XRD patterns of the SDC, BCS, and BCS–SDC powders calcined at 1000 °C for 3 h. Only diffraction peaks corresponding to SDC and BCS can be found in the pattern of the BCS–SDC composite powder. Moreover, the peaks of both SDC and BCS phases in the composite agree well with those of the single phase (Fig. 2(b)). Shown in Fig. 3 are the Raman spectra of the SDC, BCS, and BCS–SDC powders calcined at 1000 °C for 3 h obtained with a 514.5 nm laser line. The characteristic peaks at 463 cm^{-1} in SDC spectrum and 351 cm^{-1} in BCS spectrum are corresponding to F-type SDC and orthorhombic BCS, respectively. Both typical peaks can be observed in the Raman spectrum of BCS-SDC composite, and there are no shifts in the positions of these two peaks. The results of XRD and Raman analysis suggest that SDC and BCS show excellent compatibility between each other. Notably, since the composite powder was synthesized in one pot, the two different phases were mixed homogenously. Correspondingly, a uniform distribution of these two phases can be expected in the sintered membranes for SOFCs.

Fig. 4(a) shows the morphology of the BCS–SDC powders calcined at 1000 °C for 3 h. The powders, consisting of particles about 100 nm in size, agglomerate loosely together. This loose structure allows it to be easily crushed to nanometer scale powders (Fig. 4(b)),

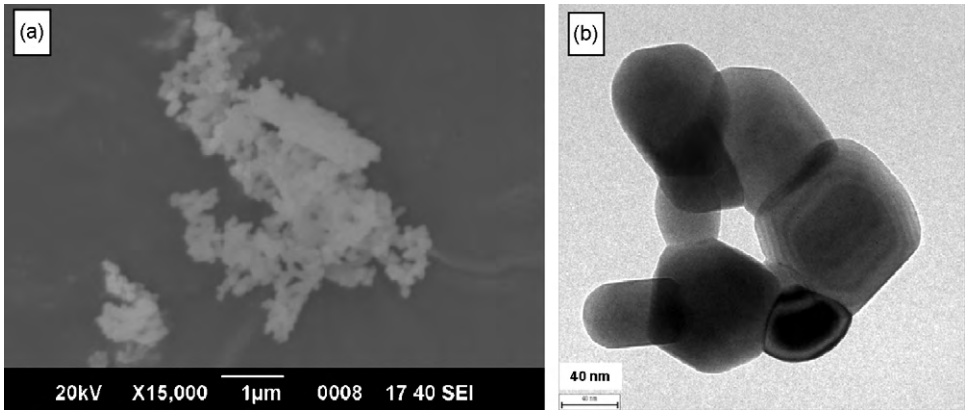

Fig. 4. SEM (a) and TEM (b) images of the BCS–SDC powder calcined at 1000 °C for 3 h.

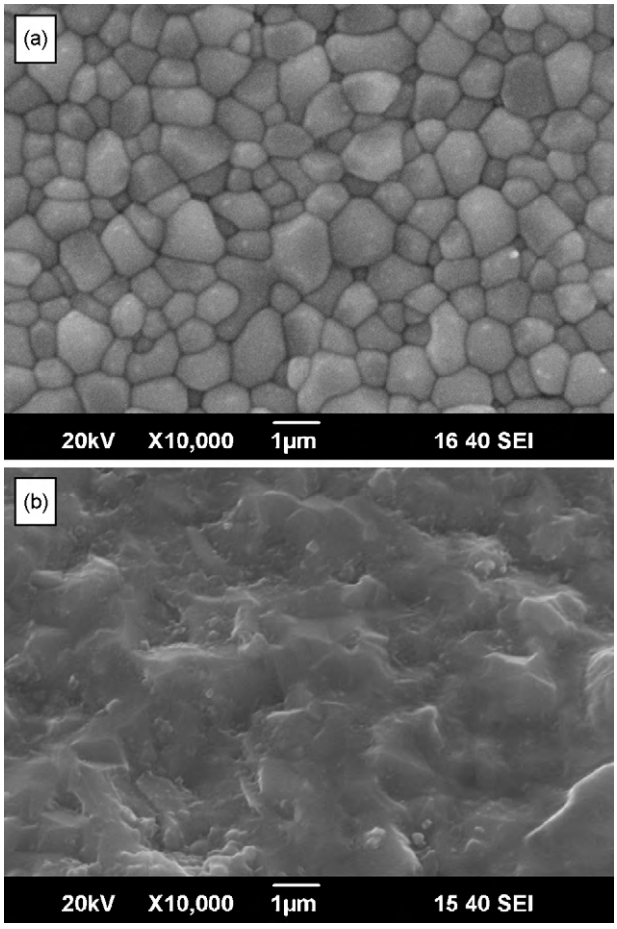

Fig. 5. SEM images of the surface (a) and cross-section (b) of the BCS–SDC electrolyte membrane sintered at 1350 °C for 5 h.

which would be beneficial to fabricate electrolyte membranes at a low temperature. Fig. 5(a) and (b) shows SEM images of the surface and cross-section of the BCS–SDC electrolyte membrane sintered at 1350 °C for 5 h, respectively. The membrane appears to be very dense and the grain size is about 1 μm, suggesting a good sintering ability of the composite powders. EDS element mapping clearly shows the presence of Ba, Ce, and Sm uniformly distributed throughout each grain in the membrane (Fig. 6), indicating that the SDC and BCS phases indeed distributed homogeneously in the composite electrolyte membrane as expected. Absolutely, the EDS results are well in accordance with the distribution scheme of the SDC and BCS crystalline grains in the electrolyte membrane as proposed earlier. The one-step gel combustion method should be responsible for the uniform distribution of the two phases, as initially the metal ions Ba^{2+}, Ce^{3+}, and Sm^{3+} were present in a homogeneous solution/gel. The results demonstrate the experimental realization of a uniform SDC–BCS double-matrix-composite electrolyte.

The electrical conductivity is a key property for materials used as an electrolyte for SOFC. To further evaluate the feasibility of the composite as an electrolyte for SOFCs, the total conductivity of the sintered (1500 °C for 5 h) BCS–SDC pellet was measured between 300 and 750 °C under different atmospheres. SEM images of the surface and cross-section fracture of the sintered pellet are shown in Fig. 7. It can be seen that the pellet was fully densified, and even no closed pores could be observed, confirming the high sintering ability of the composite. The conductivity results under different atmospheres at different temperatures are plotted in Fig. 8. A notable difference in conductivity of the sample measured in wet and dry air was observed. At temperatures below 550 °C, the conductivity under wet air (3% H_2O) was higher than that under dry air. The enhancement in conductivity under wet air was attributed to the participation of proton in the transport process [24–27]. Moreover, the hydration behavior thrives with decreasing the temperature, and hence the effect of moisture on the conductivity is

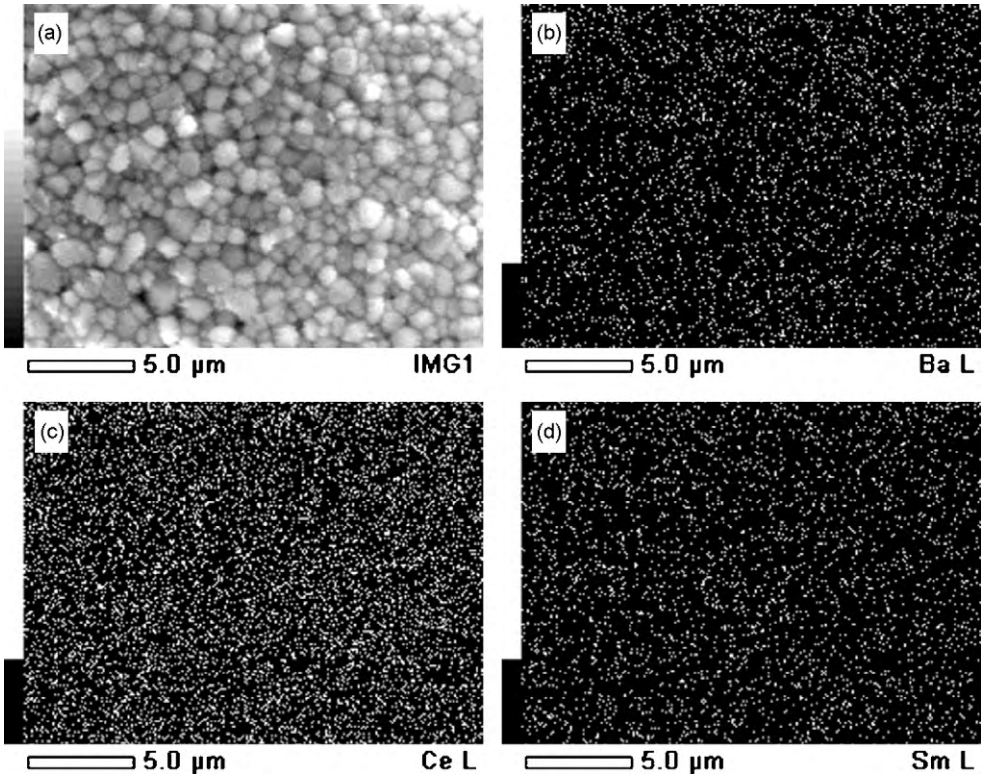

Fig. 6. SEM image of the dense BCS–SDC membrane surface (a), along with the associated EDS element mapping data of Ba (b), Ce (c), and Sm (d).

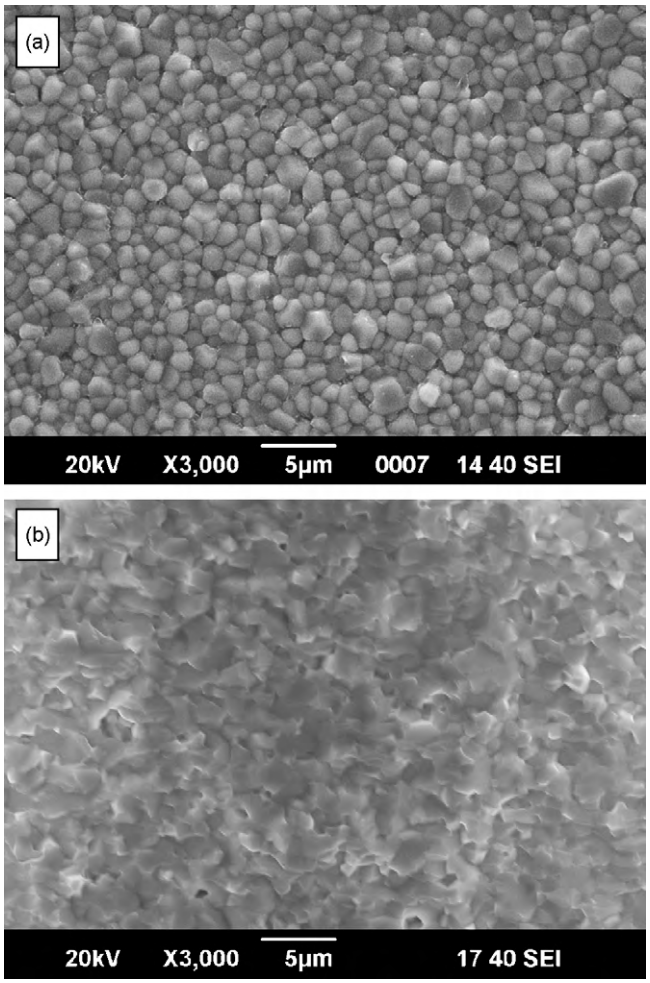

Fig. 7. SEM images of the dense BCS–SDC pellet sintered at 1500 °C for 5 h. (a) Surface. (b) Cross-section fracture.

more significant at lower temperatures. These phenomena confirmed that BCS–SDC is a mixed ionic conductor. Furthermore, the conductivity of the sample increased fleetly when the atmosphere was switched to wet hydrogen (3% H_2O) from wet air,

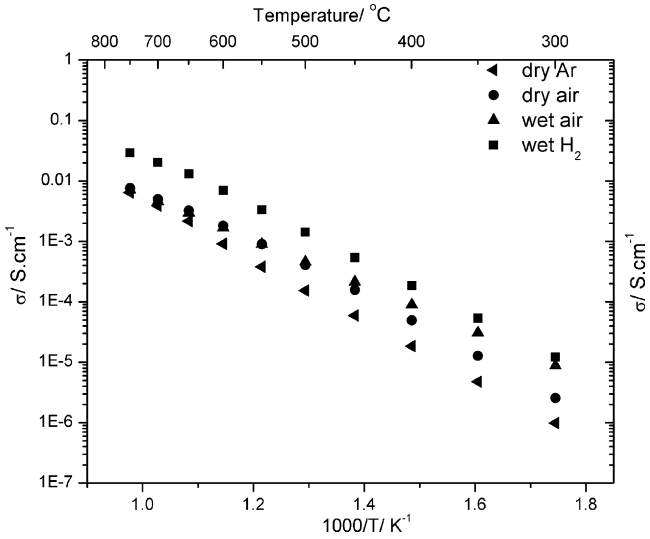

Fig. 8. Total electrical conductivity of BCS–SDC pellet sintered at 1500 °C under different atmospheres.

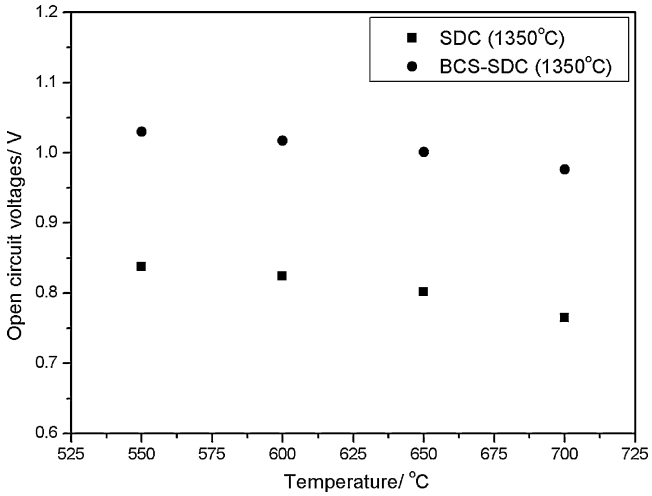

Fig. 9. The OCVs of the single cells with SDC and BCS–SDC composite as electrolyte, respectively, at different temperatures, with wet H_2 (3% H_2O) as the fuel and static air as the oxidant.

especially at elevated temperatures. In wet air, the conductivity was only 4.60×10^{-3} and 8.82×10^{-6} S cm^{-1} at 700 and 300 °C, respectively; while it increased to 2.04×10^{-2} and 1.21×10^{-5} S cm^{-1} in wet hydrogen at the same temperatures, respectively. Notably, the total conductivity was comparable with that of the state-of-the-art proton conductor $BaZr_{0.1}Ce_{0.7}Y_{0.2}O_{3-\delta}$ (BZCY) [5]. In addition, the conductivity in dry air was higher than that in dry argon, and the conductivity enhancement can be ascribed to the electronic conduction coming from the holes [24].

The OCVs of button cells at different operating temperatures using SDC or BCS–SDC composite as the electrolyte were compared to confirm the electronic current-blocking ability of BCS–SDC, as shown in Fig. 9. The OCV values with SDC electrolyte were only 0.765, 0.802, 0.824, and 0.838 V at 700, 650, 600, and 550 °C, respectively, due to the well-known partial internal shorting under the reducing atmosphere [15,18]. In contrast, the OCVs increased drastically when BCS was incorporated with SDC forming the composite electrolyte, achieving 0.976, 1.001, 1.017, and 1.030 V at 700, 650, 600, and 550 °C, respectively. The great enhancement of OCVs revealed that the electronic current through the electrolyte membrane was effectively and mostly blocked. As expected initially, the SDC grains were effectively protected from reduction by the BCS matrix in the composite electrolyte and hence the electronic conduction in the composite electrolyte was greatly suppressed, resulting in higher OCV values. Nevertheless, the OCVs are still a bit lower than those of the cells with typical YSZ [28,29] or doped $BaCeO_3$ [5,8,23] electrolytes, confirming that there is still a little electronic conduction in BCS–SDC (Fig. 8).

Besides the improvement of OCVs over SDC, BCS–SDC composite also exhibits a higher stability than BCS. The stability of BCS–SDC electrolyte membrane was also evaluated under fuel cell testing conditions, and for the sake of demonstrating its actual stability, the stability of BZCY electrolyte membrane, which is admittedly high [5], was also investigated for comparison. The OCVs of the two samples at 650 °C were recorded as a function of operation time when hydrogen was used as the fuel, as shown in Fig. 10. As seen in Fig. 10(a), the OCV of the cell with BZCY membrane dropped from 1.023 to 0.987 V after 50 h, declining about 3.52%. In contrast, when BCS–SDC was used as the electrolyte membrane, the OCV appeared more stable (Fig. 10(b)) and only declined 0.99% after 95 h. The stability of OCV further confirmed the fact that the chemical stability of BCS–SDC was highly improved after introducing the SDC matrix. As mentioned above, the SDC matrix in the

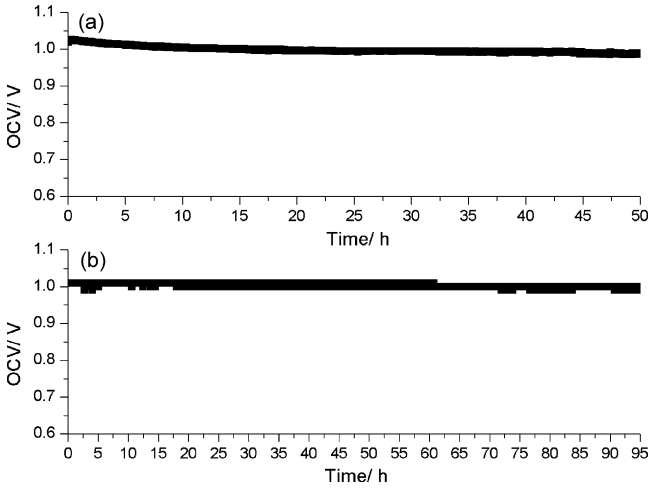

Fig. 10. The OCV of the single cells based on BZCY (a) and BCS–SDC (b) composite electrolyte at 650 °C as a function of time with wet hydrogen (3% H_2O) as the fuel.

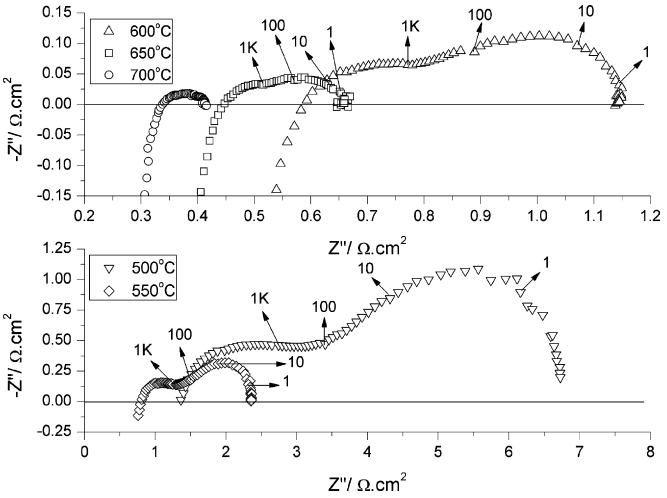

Fig. 12. Impedance spectra of the tested cell measured under open current conditions at different temperatures, and the numbers are the frequencies in hertz.

composite acted as a covering layer for the BCS crystalline grains here, and this covering layer kept the BCS grains away from corrosion caused by CO_2 and H_2O, leading to a higher chemical stability correspondingly.

Determinately, compared to the single-phase electrolyte material, the electronic conduction is effectively suppressed and the chemical stability is apparently improved for the BCS–SDC composite electrolyte. The exciting results demonstrate that, in addition to exploring materials with completely new structures or components, to amalgamate the different classical material systems into composite might also be an effective method. The above experiments verify a new interesting route to develop novel functional composite electrolytes to meet demands of various applications. Correspondingly, this concept can also be expanded to the investigation of other functional materials.

In order to assess the electrochemical performance of the button cells based on BCS–SDC composite electrolyte, Ni-BCS–SDC anode-supported button cells with a 30-μm-thick BCS–SDC electrolyte membrane fabricated at 1350 °C, combining a $Sm_{0.5}Sr_{0.5}CoO_{3-\delta}$–$Ce_{0.8}Sm_{0.2}O_{2-\delta}$ (SSC–SDC) cathode, were tested using wet H_2 as the fuel and static air as the oxidant. Shown in Fig. 11 are the *I–V* and power density curves of a button cell at different temperatures. The OCVs were 0.940, 0.971, 0.994, 1.014, and 1.034 V, and the peak power densities were 505, 345, 216, 123, and 61 mW cm^{-2} at 700, 650, 600, 550, and 500 °C, respectively. In addition, the power densities measured at a cell voltage of 0.7 V achieved 404, 283, 185, 86, and 48 mW cm^{-2} at 700, 650, 600, 550, and 500 °C, respectively. The OCVs are a bit lower than those discussed above, which might be induced by the gas leakage through the sealing region. It should be noted that the power densities can be further improved by optimizing the anode microstructure with pore-creating materials [30].

The electrochemical impedance spectra of the button cell measured under open current conditions are shown in Fig. 12. The intercept with the real axis high frequencies represents the ohmic resistance (R_{ohm}) of the cell, which includes ionic resistance of the electrolyte, contact resistance associated with the interface, and electronic resistance of the electrodes and Ag wires, whereas the difference between the high frequency and the low frequency intercept with the real axis represents the polarization resistance (R_p) of the cell [5]. Obviously, both R_{ohm} and R_p dramatically decreased as increasing the operating temperature. Fig. 13 shows R_{ohm} and R_p of the tested button cell at different temperatures, and the ratio of $R_{ohm}/(R_{ohm}+R_p)$ is inserted in Fig. 13. The resistances were estimated from impedance spectroscopy measured under open circuit

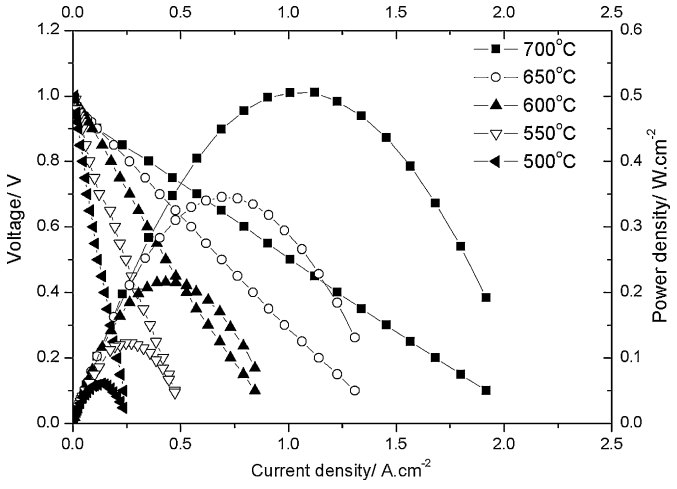

Fig. 11. *I–V* and power density curves of the Ni-BCS–SDC|BCS–SDC|SSC–SDC single cell at different temperatures with wet hydrogen (3% H_2O) as the fuel and static air as the oxidant.

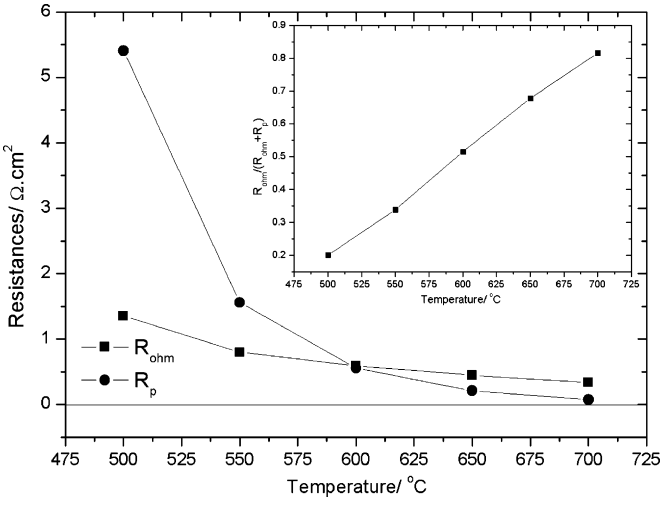

Fig. 13. The ohmic resistances (R_{ohm}) and polarization resistances (R_p) of the testing button cell estimated from impedance spectroscopy under open circuit conditions at different temperatures. Inset: the ratio of $R_{ohm}/(R_{ohm}+R_p)$ at different temperatures.

conditions. R_{ohm} were 0.337, 0.446, 0.587, 0.798, and 1.354 $\Omega\,cm^2$, and R_p were 0.076, 0.212, 0.552, 1.558, and 5.407 $\Omega\,cm^2$ at 700, 650, 600, 550, and 500 °C, respectively. It can be observed that, at temperatures higher than 600 °C, R_{ohm} was predominant, accounting for 0.515, 0.678, and 0.816 at 600, 650, and 700 °C, respectively. Nevertheless, R_p increased much faster than R_{ohm} with the temperature decreasing. Consequently, R_p was predominant in the total cell resistance at 550 and 500 °C, accounting for about 0.661 and 0.800. That is to say, at temperatures higher than 600 °C, the performance of the cell based on BCS–SDC electrolyte was mainly limited by R_{ohm}, while, at low temperatures, the performance was limited by R_p. Similar results were observed in button cells based on other electrolytes [31,32]. The rapid increase of the polarization resistance at low temperatures is very likely correlative with the configuration of the cell, especially the electrode microstructures. Therefore, besides thinning the electrolyte membrane, which would decrease R_{ohm} of the cell, the electrode microstructure of the cell should also deserve further improvement in order to attain higher electrochemical performances, especially at reduced temperatures.

4. Conclusions

In summary, the present work demonstrated that an electronic current-blocked stable mixed ionic (oxygen ions and protons) conductor can be obtained by combining BCS and SDC with a weight ratio of 1:1 via a one-step gel combustion method. BCS and SDC crystalline grains distributed uniformly throughout each grain in the composite. The new double-matrix configuration ionic conductor avoids the typical drawbacks of BCS and SDC, showing not only a very high chemical stability but also much higher OCVs than SDC under the fuel cell conditions. Moreover, the composite showed a remarkable total conductivity of 0.0204 $S\,cm^{-1}$ at 700 °C in wet hydrogen. Besides, it can be expected that the double-matrix-composite electrolyte might still be achieved after reducing the account of BCS or SDC on the premise that BCS or SDC powders are in much smaller sizes. Using the BCS–SDC composite electrolyte, a button cell with a Ni-BCS–SDC cermet anode and a SSC–SDC composite cathode exhibited good performances with wet hydrogen as the fuel, and the peak power density achieved 505 $mW\,cm^{-2}$ at 700 °C. Resistances of the testing cell revealed that, at temperatures higher than 600 °C, the performance of the cell was limited by the ohmic resistance, while, at lower temperatures, the performance was limited by the polarization resistance of the cell. The interesting experimental results mentioned above offer a novel way to explore practicable functional materials in future investigations.

Acknowledgments

This work was supported by National High-tech R&D Program of China (No. 2007AA05Z157) and Key Program of Chinese Academy of Sciences (No. KJCX1.YW07). W.P. Sun also acknowledges the CAS Special Grant for Postgraduate Research, Innovation and Practice.

References

[1] T.H. Etsell, S.N. Flengas, Chem. Rev. 70 (1970) 339.
[2] E.C. Subbarao, H.S. Maiti, Solid State Ionics 11 (1984) 317.
[3] J.B. Goodenough, Annu. Rev. Mater. Res. 33 (2003) 91.
[4] K.D. Kreuer, Annu. Rev. Mater. Res. 33 (2003) 333.
[5] C.D. Zuo, S.W. Zha, M.L. Liu, M. Hatano, M. Uchiyama, Adv. Mater. 18 (2006) 3318.
[6] L. Yang, S.Z. Wang, K. Blinn, M.F. Liu, Z. Liu, Z. Cheng, M.L. Liu, Science 326 (2009) 126.
[7] Y. Ma, X.D. Wang, S.H. Li, M.S. Toprak, B. Zhu, M. Muhammed, Adv. Mater. 22 (2010) 1.
[8] L. Yang, C.D. Zuo, S.Z. Wang, Z. Cheng, M.L. Liu, Adv. Mater. 20 (17) (2008) 3280.
[9] S. Banerjee, P.S. Devi, D. Topwal, S. Mandal, K. Menon, Adv. Funct. Mater. 17 (2007) 2847.
[10] B.R. Sneha, V. Thangadurai, J. Solid State Chem. 180 (10) (2007) 2661.
[11] F. Trobec, V. Thangadurai, Inorg. Chem. 47 (19) (2008) 8972.
[12] J.W. Fergus, J. Power Sources 162 (2006) 30.
[13] K. Eguchi, T. Setoguchi, T. Inoue, H. Arai, Solid State Ionics 52 (1992) 165.
[14] R. Doshi, V.L. Richards, J.D. Carter, X.P. Wang, M. Krumpelt, J. Electrochem. Soc. 146 (1999) 1273.
[15] B.C.H. Steele, Solid State Ionics 129 (2000) 95.
[16] A. Atkinson, Solid State Ionics 95 (1997) 249.
[17] T. Hashida, K. Sato, Y. Takeyama, T. Kawada, J. Mizusaki, ECS Trans. 25 (2009) 1565.
[18] X.G. Zhang, M. Robertson, C. Deces-Petit, W. Qu, O. Kesler, R. Maric, D. Ghosh, J. Power Sources 164 (2007) 668.
[19] S.V. Bhide, A.V. Virkar, J. Electrochem. Soc. 146 (1999) 2038.
[20] F.L. Chen, O. Toft Sørensen, G.Y. Meng, D.K. Peng, J. Mater. Chem. 7 (1997) 481.
[21] C.-S. Tu, R.R. Chien, V.H. Schmidt, S.-C. Lee, C.-C. Huang, C.-L. Tsai, J. Appl. Phys. 105 (2009) 103504.
[22] L. Bi, S.Q. Zhang, S.M. Fang, Z.T. Tao, R.R. Peng, W. Liu, Electrochem. Commun. 10 (2008) 1598.
[23] W.P. Sun, L.T. Yan, B. Lin, S.Q. Zhang, W. Liu, J. Power Sources 195 (10) (2010) 3155.
[24] F.L. Chen, O. Toft Sørensen, G.Y. Meng, D.K. Peng, J. Eur. Ceram. Soc. 18 (1998) 1389.
[25] J. Guan, S.E. Dorris, U. Balachandran, M. Liu, Solid State Ionics 100 (1997) 45.
[26] K.E.J. Eurenius, E. Ahlberg, I. Ahmed, S.G. Eriksson, C.S. Knee, Solid State Ionics 181 (2010) 148.
[27] E. Ruiz-Trejo, J.A. Kilner, J. Appl. Electrochem. 39 (2009) 523.
[28] R.Q. Yan, D. Ding, B. Lin, M.F. Liu, G.Y. Meng, X.Q. Liu, J. Power Sources 164 (2007) 567.
[29] H.Q. Wang, W.J. Ji, L. Zhang, Y.H. Gong, B. Xie, Y.S. Jiang, Y.Z. Song, Solid State Ionics, in press.
[30] T. Suzuki, Z. Hasan, Y. Funahashi, T. Yamaguchi, Y. Fujishiro, M. Awano, Science 325 (2009) 852.
[31] W.P. Sun, L.T. Yan, Z. Shi, Z.W. Zhu, W. Liu, J. Power Sources 195 (15) (2010) 4727.
[32] W.P. Sun, Z. Shi, S.M. Fang, L.T. Yan, Z.W. Zhu, W. Liu, Int. J. Hydrogen Energ. 35 (15) (2010) 7925.